

Assessment of Coastal Water Quality by Testing a Linear Model Using Landsat 8 SST Data: Exploratory Study

YOUSRA EZZGHARI

Abdelmalek Essaâdi University, Morocco

yousra.ezzghari@etu.uae.ac.ma

EL KHALIL CHERIF

Instituto Superior Técnico, Portugal

National Institute of Oceanography and Applied Geophysics, Italy

c.elkhalil@uae.ac.ma

AYMAN BNOUSSAAD

Instituto Superior Técnico, Portugal

aymanbnoussaad@gmail.com

HAMZA EL AZHARI

Abdelmalek Essaâdi University, Morocco

hamza.elazhari@etu.uae.ac.ma

HAKIM BOULAASSAL


Abdelmalek Essaâdi University, Morocco

h.boulaassal@uae.ac.ma

The Mediterranean Basin, off the coast of Tangier, Morocco, is one of the most valuable seas, because of the diversity of its ecosystem. However, pollution has become a growing issue along this coast recently. For this reason, we tested a linear model developed for the Atlantic western coastal waters of Tangier using sea surface temperature (SST) estimated from Landsat 8 images and *Escherichia coli* concentration (*E. coli*) in-situ measurement to determine the Mediterranean northern coastal waters quality of Tangier in 15 Selected Sites (SS1 to SS15) along the coast from Tangier to Ksar-Sghir. In addition, descriptive statistics, and geographic information systems (GIS) were employed to explore the spatial association of the data. The results indicate that the SST and *E. coli* distributions have the highest values in the SS4-SS13 and SS15 due to the Souani and Mghogha rivers and Tangier Med Port, reflecting poor quality and a very high level of dangerous contam-

ination in this area. The SS1, SS2, SS3, and SS14 reflected low levels of SSTs and E. coli concentrations thus, medium, and good-quality water is present around the cities of Tangier and Ksar-Sghir. The relationship between water temperature and E. coli concentration showed a high correlation coefficient, 80% (RMSE = 0.8), while the IDW, helped frame the pollution zone along the shore. Although only values near the shore are valid, the values deeper in the Gibraltar Strait were extrapolated due to the absence of data points at depth. This IDW results showed the negative impact of discharges from estuaries and maritime traffic. As a result, the tested model is useful for estimating the quality of coastal water on the Mediterranean side of Tangier, and in the future, as a means of potentially monitoring pollution in this region.

Key Words: Mediterranean waters, Escherichia Coli, Landsat 8, SST, quality water, Gibraltar Strait

 <https://emuni.si/ISSN/2232-6022/16.251-280.pdf>

INTRODUCTION

The coastal waters offer some of the best landscape areas (Yi et al. 2022; Gravari-Barbas and Jacquot 2018) and serve other important purposes, such as marine aquaculture, commercial navigation, or as a repository for sewage and industrial waste (Cherif, Salmoun, and Mesas-Carrascosa 2019). Such activities are not always compatible with each other nor the population that lives along the coastal zone, which represents 40 percent of the total population (Maul and Duedall 2019; Sloggett et al. 1995). Furthermore, the expansion of these activities has a serious impact in the environment, putting human health and aquatic life habitats at risk (Lamghari Moubarrad and Assobhei 2005). For sustainable coastal water, water resource management and constant monitoring are required. Furthermore, water treatment requires an awareness of the quality of the water body. Water quality considers the thermal and biological characteristics of a body of water. It is used as an index to determine the suitability of water. Defining seawater quality can be difficult as its usage varies widely (Gong et al. 2019). Remote sensing is widely used for land cover and land use classification and has been shown to be ef-



ficient for use in heterogeneous mesh segmentation (Gómez 2003; Sertel et al. 2022), but water bodies have proven difficult to map due to their homogeneity and high variability in reflectance, and a number of satellite remote sensing products for water resources management are still in their infancy (Yang et al. 2022; Sheffield 2018; Gholizadeh 2016). Nevertheless, there is tremendous potential for the use of remote sensing imagery for monitoring and assessing water quality (Cherif et al. 2020). Relying on the spectral properties of water leaving radiance, it is possible to remotely determine and quantify water quality parameters (Bourouhou and Salmoun 2021b).

[253]

Sea surface temperature was one of the first ocean variables to be studied from earth observation satellites, and the satellite instruments to retrieve and estimate these SSTs have undergone over a half century of development (Cherif, Salmoun, and Mesas-Carrascosa 2019; Govekar et al.; Amani et al. 2022). The SST parameter has demonstrated its association with many bacterial concentrations. For instance, in the infamous John Snow cholera case in London, it was discovered that sea surface temperature, retrieved from satellite imagery, showed an annual cycle similar to the cholera case data collected from 1992 to 1995 in Bangladesh (Alparslan et al. 2007). This association was later confirmed for other bacterial concentrations, such as *E. coli*, with a high correlation coefficient ($R^2 = 0.85$) (Anding and Kauth 1970).

The traditional way to calculate *E. coli* concentrations consists of collecting samples from the site and analyzing them in a laboratory. The results in this case are highly explicit (Cherif et al. 2020; Sikder et al. 2021). In marine environments, *E. coli* concentration is considered a fundamental parameter of water quality and is used to monitor fecal coliforms (FC) (Odonkor and Mahami 2020; Brando and Dekker 2003). However, although effective, this conventional method is also costly and time-consuming (El-Din et al. 2013). Furthermore, in-situ measurements are sometimes inconsistent and proved to be difficult to use to assess water quality, especially in large areas. Hence, since the 1970s, many researchers have applied remote sensing techniques to assess water quality (Anding and Kauth 1970; Topp et al. 2020; Giardino et al. 2014).

Remote sensing has been applied to monitor different water bodies, such as coasts, lakes, and artificial ponds (Doña et al. 2016; Peng et al. 2022; Hadjimitsis and Clayton 2009). Many of these study areas suffer from different quantitative computational problems. However, the application of remote sensing imagery in forecasting and water quality assessment is progressively improving (Alparslan et al. 2007). The main water quality parameters under consideration are the core objective of many of these studies, such as sea surface temperature (SST), turbidity, chlorophyll-a, Secchi depth, dissolved oxygen, and others. These parameters can be used to determine other water concentrations, such as, in our case, *E. coli* concentrations, based on thermal data derived from satellite or drone imagery (Konratyev et al. 1998). The assessment and predictive capability of the developed models are highly argued. Naturally, the accuracy of *E. coli* concentration estimation captured by small unmanned aerial vehicles (SUAV or drone) is higher than the satellite-based imagery due to its higher resolution (Topp et al. 2020; Giardino et al. 2014).

Our study area is on the northern coast of Morocco, in a Mediterranean region that has historically been a high-traffic volume area with three main estuaries: Oued El Maleh, Oued Lihoud, and Oued Souani (Er-Raioui et al. 2012). Furthermore, the Strait of Gibraltar plays a crucial role in controlling all exchanges and modifications of the biogeochemistry of the marine ecosystem and the circulation between the Mediterranean Sea and Atlantic Ocean (Maillard and Santos 2008). The bathing waters of this coast are particularly frequented by both locals and tourists, which raises concerns considering the health risks.

More than 40% of the world's population lives in coastal areas and along lake or river shores (Cherif et al. 2020). Therefore, any changes in aquatic ecosystems due to human, urbanization, industrial, or touristic activities have grave effects on these areas. Tangier Ksar-Sghir, located on the Moroccan coast at the western entrance to the Strait of Gibraltar, has experienced significant demographic growth and increased industrial activity in recent years, particularly since the new Tangier Med port began service in 2016. This situation directly affects the quality of the coastal water in this region.



Brando et al. (2003) adopted a linear model based on thermal data from Landsat 8 and in-situ measurements of *E. coli* to estimate the water quality on the western coast of Tangier, Morocco. Their results showed a significant correlation between log *E. coli* and the temperature difference between water and air.

[255]

The aim of the present work is twofold. First, it describes the performance of testing a linear equation to estimate the concentration of *E. coli* and the water quality in the Tangier Mediterranean coast (Tangier Ksar-Sghir coastal water). Second, it demonstrates the potential of using remote sensing as an early and effective warning system for coastal water pollution using statistical analysis and GIS.

MATERIALS AND METHODS

Study Area

Tangier Ksar-Sghir coastal water (figure 1) is located in the Strait of Gibraltar between the Mediterranean Sea and the Atlantic Ocean. The coast is famous by its proximity to the capital of northern Morocco, Tangier. Tangier, an area of 17 262 km², representing 2.43% of the total area of the Moroccan Kingdom. Over 40 km is comprised of the village of Ksar-Sghir, which covers an area of 50,000 m². This region is well known by Tangier Med Port (Ben Ali and Mahacine 2022). It is a significant link to more than 180 ports in 70 countries and due to its geographical position, it is known as the second busiest sea lane in the world, with more than 100,000 boats per year (El-Din et al. 2013).

The region's climate varies from sub-humid Mediterranean in the mountains to semi-arid along the coastal strip. It is strongly influenced by the Atlantic Ocean, the Mediterranean Sea and the relief (Haut Commissariat au Plan 2020). Due to altitude, latitude and ocean, the climate of study area presents a strongly heterogeneity. The annual average rainfall varies between 400 mm and 700 mm depending on altitude. In general, the temperature remains mild in winter, soft in summer as well on the coasts as in altitude. Moreover, due to geographical localization of Tangier Ksar-Sghir, the coastal area is very windy thanks to coastal currents (East or West) that rush through the Gibraltar lane.

[256]

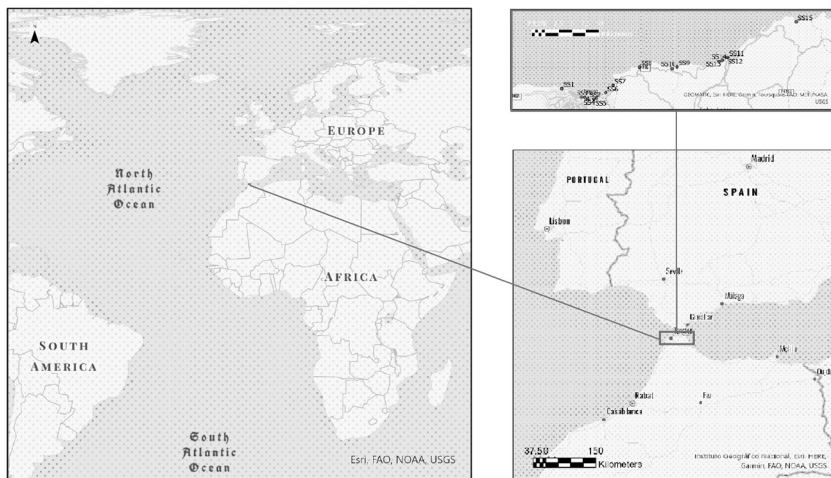


FIGURE 1 Situation Map of the Study Area

The Tangier Ksar-Sghir is particularly affected by the negative consequences of climate change and marine pollution. It has experienced, in recent decades, a variety of pressures from increasing urbanization. According to the last census in 2015, it had 1,065,601 inhabitants (Bouramtane et al. 2021). Moreover, the coastline between Tangier Ksar-Sghir is characterized by intense port activity based mainly at the level of the Tangier Med Port complex (commercial port) and the port of the city of Tangier (Ben Ali and Mahacine 2022). In terms of industrial activities, most of the industrial units are located along the coastline (Doney 2010). This represents a type of severe impact due to the discharge of liquid effluents into the sea. Additionally, fishing activities and seaside tourism cause pressure on marine ecosystems and have a negative impact on water quality in this region, respectively (Islam and Tanaka 2004).

Selected Sampling Point

In the last few years, the Tangier-Ksar-Sghir region has undergone a significant evolution in terms of industrial, economic, and touristic activities. The main objective of this investigation is to frame the study area and determine the ideal sampling points that will provide a fair estimation of the bacterial propagation of *E. coli*.



TABLE 1 Selected Sites with Their Geographical Coordinates

SS1	Marqala	SS6	Ghandouri	SS11	Ksar-Sghir
SS2	Tangier city	SS7	Lamrissat	SS12	Port Tangier Med
SS3	Tangier city	SS8	Sidi Kanqouch	SS13	Port Tangier Med
SS4	Tangier Malabata	SS9	Oued Aliane 1	SS14	Port Tangier Med
SS5	Tangier Malabata	SS10	Oued Aliane2	SS15	Oued el Marsa

[257]

In this study, the sampling waters were collected in 2017 at 15 different locations (three samples were collected at each location) for bacteriological parameters. The sampling stations were chosen with uniform spacing and little variation, and were based on the geographical conditions, accessibility, and the most known sites for human activities (urbanism, industry and tourism) and materials of sampling (it is not according to work in depth). Table 1 illustrates the geographical coordinates of each site.

Study Procedure

In this study, the water quality in the Tangier-Ksar-Sghir area was analyzed using data from Landsat 8 images (Thermal Infrared Sensor) and based on the in-situ measurements of E. coli concentrations provided by Bourouhou and Salmoun (2021a). We used a methodology for estimating the concentration of E. coli on the northern coast of Tangier, which was previously used on the Atlantic western cost of Tangier and proved efficient (Cherif et al. 2020).

The statistical approach was conducted in order to analyze and compare the in-situ and estimated data to see if they behaved similarly. The descriptive statistics, the correlation matrix, and the scatterplots are produced using Excel. The use of the spatial aspect of the sites is accomplished through data posting, using arcGIS software to graphically investigate our dataset and gain a better understanding of it.

Sea Surface Temperature Data

The Landsat 8 (L8) satellite can continuously provide a significant volume of data for all landmasses and near-coastal areas on earth with high performance and quality (Bradtke 2021; Wu et al. 2019).

Landsat 8 has two bands of TIRS. The TIRS sensor provides image data for two thermal bands: Band 10 (B10) and Band 11 (B11) with high spatial resolution (100 m), and wavelength (10.0–12.5 μm) (Amani et al. 2022).

[258] The atmosphere between the satellite and the earth's surface consists of various gases that absorb and/or scatter both incident and reflected sunlight (Grau and Gastellu-Etchegorry 2013). The Landsat instruments do not contain on-board sensors to measure these conditions, so this information is obtained through other observations, called auxiliary data (US Geological Survey 2023b).

More recently, however, the United States Geological Survey aims to improve the Landsat products to prevent this natural reaction and to support Earth's change studies (Roy et al. 2014). Therefore, it has initiated an effort to create a collection of Landsat Level 2 Science Products (L2SP) (Galve et al. 2022). It requires the atmospheric auxiliary data from multiple external sources for surface temperature data processing (Banzon et al. 2016; Donlon et al. 2012). For this, Advanced Spaceborne Thermal Emission and Reflection Radiometer Global Emissivity Dataset (ASTER GED) data are used by the Surface Temperature (ST) algorithm in order to obtain the emissivity auxiliary data. Additionally, for the atmospheric correction, the Goddard Earth Observing System Model, Version 5 (GEOS-5) Forward Process for Instrument Teams (FP-IT) data is used in the Single Channel algorithm (US Geological Survey 2023b). It's important to note that the Single Channel algorithm that generates the ST band requires L1's TIRS Band 10 as an input (US Geological Survey 2023a). Additional details describing the auxiliary file structures can be found on the US Geological Survey website (US Geological Survey 2023a).

The Landsat Level-2 products are derived from the corresponding Level-1 products and additional corrections are applied to remove their temporally, spatially and spectrally varying atmospheric effects (Teixeira Pinto et al. 2020). Compared to the Level 1 products, which the Digital Number (DN) is converted to Top-of-Atmosphere (TOA) through the radiometric calibration process and then into TOA Brightness Temperature, the Level 2 products are atmospher-



TABLE 2 TIRS Images for SST Estimated Details (Path/Row 201/35, B10, and Level2)

LC08_L2SP_201035_20170423_20200904_02_T1
LC08_L2SP_201035_20170626_20200903_02_T1
LC08_L2SP_201035_20170728_20200903_02_T1
LC08_L2SP_201035_20170914_20200903_02_T1
LC08_L2SP_201035_20171117_20200902_02_T1
LC08_L2SP_201035_20171219_20200902_02_T1

[259]

ically corrected data (Teixeira Pinto et al. 2020). More information on Landsat 8 Level 2 Science Products (L2SP) band specifications can be found on the US Geological Survey official website (US Geological Survey 2023b).

In this research, the SST values are derived from the Collection 2 Level 2 Science Product (L2SP) B10 Thermal Infrared Sensors (TIRS). Six images covering the Tangier Ksar-Sghir area from 2017 were uploaded (table 2). To achieve a high accuracy of light reflectance from the Earth’s surface, cloudy images were not included.

Once the Landsat 8 thermal band (B10) images were downloaded, the estimated SST values corresponding to our points of interest were computed using the Sentinel Application Platform (SNAP) software developed by the European Space Agency (ESA) (Ramdani et al. 2021; Ritchie et al. 2003).

To do this, we first started by converting the temperature values from Kelvin to Celsius. The selected sites were imported according to their geographical coordinates to extract the sea surface temperature of each point using pinning tools, and then the selected pins were exported. The following flowchart presented in figure 2 illustrates the process followed to extract sea surface temperature (SST) from Landsat8 B10.

Water Quality Estimation

In this part of our study, a total of 15 sites were selected from the total concentration in-situ measurements and are available. After deriving the in-situ data from the year 2017 (Bourouhou and Salmoun 2021b), we matched the data with the SSTs and Air Temperatures

[260]

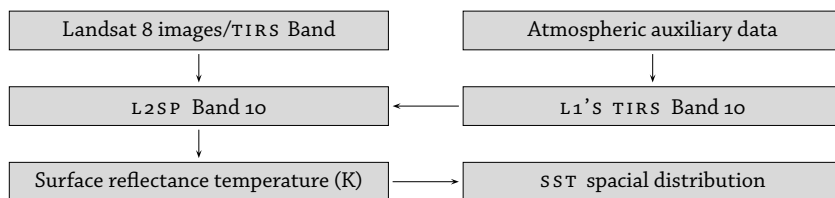


FIGURE 2 Flowchart for Extracting Sea Surface Temperature from Landsat8 B10

TABLE 3 Quality Classes According to Moroccan Norm NM 03.7.200

Quality classes	A (good quality)	B (medium quality)	C (temp. polluted)	D (poor quality)
E. coli (UFC/100 mL)	≤150	≤250	≤500	≥500

(ATS) of the same date. The concentrations of E. coli in Tangier Ksar-Sghir were determined based on the linear model of (Cherif et al. 2020).

$$y = 0.37x + 2.4,$$

where $x = SST - AT$, and $y = \log_{10} [E. coli (UFC/100 mL)]$.

As previously mentioned, the SST values of each point were derived from band 10 of TIRS images. The Air Temperature (ATS) was obtained from the Tangier Ibn Batouta airport weather station (Seyhan and Dekker 1986). See Table 3 for further information. The water quality class of each selected site was assigned according to Moroccan quality standards (Moroccan norm NM 03.7.200), represented in table 3 (Mahjoubi 2019; Usali and Ismail 2010).

RESULTS AND DISCUSSION

Exploring the potential of remote sensing for estimating water temperature has drawn many authors to using satellite imagery for this purpose in various regions around the world (Giardino et al. 2014; Wang and Ma 2001; Pyo et al. 2016; Morgan et al. 2020; Cheng et al. 2022) and in Morocco's northern waters (Anding and Kauth 1970; Brando and Dekker 2003; El-Din et al. 2013). We tested a linear equation to determine E. coli concentrations using existing SST and





[261]

FIGURE 3 Location of the Two Statistical Anomalies in the Study Area

Air Temperature data from several locations in the Mediterranean coastal water of Tangier (Anding and Kauth 1970). This equation allowed for the estimation of *E. coli* concentrations along Tangier's Ksar-Sghir region's coastline in 2017.

Exploratory Data Analysis

Table 4 summarizes the results of the in-situ measurements (sea surface temperature, *E. coli* concentration, water quality class, and air temperature for each selected site (El-Din et al. 2013; Ritchie et al. 2003) and estimated quantities (sea surface temperature extracted from band 10 of Landsat 8, the concentration of *E. coli* estimated from the equation (Vanhellemont 2020), and water quality classes (Mahjoubi et al. 2019; Usali and Ismail 2010)).

The estimated water quality classes showed medium to high correlation with in-situ measurements, SS1 and SS6 having relatively lower correlation. The bathing water in SS1 was classified as class B instead of D; this fluctuation can be explained by the presence of the pre-treatment station near the first site (figure 3), that spills periodically. The SS2 and SS3 were classified as good quality (class A) for both in-situ and estimated variables. On the other hand, SS4 and SS5, were class D, C and D, D in-situ and estimated respectively, due to the rejection of the estuary of Souani and Mghogha rivers. The selected sites from SS6 to SS13 were characterized by poor quality water (class D), which reflects a very high level of dangerous contam-

TABLE 4 Bacteriological Results of the Concentration of E. Coli Estimated, Sea Surface Temperature Estimated (SST) and Water Quality Classes

Sites	(1)	(2)	(3)	(4)	(5)	(6)	(7)	(8)	(9)
SS1	27.227	27.267	35.622	-0.040116	2.385157	880	242.75	D	B
SS2	22.333	24.254	24.971	-1.921053	1.689210	14	48.89	A	A
SS3	21.277	24.254	24.930	-2.977190	1.298440	20	19.88	A	A
SS4	17.482	16.259	16.310	1.223160	2.852569	920	712.15	D	D
SS5	16.259	16.259	17.226	-0.000028	2.399990	530	251.18	D	C
SS6	16.210	16.259	17.339	0.049475	2.381694	79	240.82	A	D
SS7	30.024	27.267	35.181	2.757278	3.420193	4500	2631.44	D	D
SS8	26.445	24.254	21.926	2.190744	3.210575	1361	1623.96	D	D
SS9	29.752	27.658	32.272	2.094201	3.174854	1871	1495.73	D	D
SS10	26.571	24.254	24.127	2.317000	3.257290	1870	1808.38	D	D
SS11	30.066	27.658	31.708	2.408324	3.291080	1709	1954.70	D	D
SS12	24.436	24.425	24.883	0.011684	2.404323	176	253.70	B	C
SS13	26.832	24.425	27.439	2.406600	3.290442	263	1951.83	C	D
SS14	17.838	18.314	13.039	0.475758	2.223970	22	167.48	A	B
SS15	20.461	18.314	19.636	2.153018	3.196617	1500	1572.59	D	D

NOTES Column headings are as follows: (1) SST (°C), (2) AT (°C), (3) SST B10 (°C), (4) X (°C), (5) Y (°C), (6) [E. coli] in-situ (UFC/100 mL), (7) [E. coli] estimated (UFC/100 mL), (8) water quality class (in-situ), (9) water quality class (estimated).

ination in this region, which hosts several resorts and public beaches (figure 3). Furthermore, it represents a significant concentration of E. coli. This high concentration of E. coli indicates that the environment is suitable for its survival. According to an environmental impact study carried out by Tangier Mediterranean Spatial Agency (TMSA) (2010), the presence of fecal bacteria (E. coli) could be due to rejections from ships (marine traffic) (US Geological Survey 2019). SS14 was classified as class A and estimated at B, and in SS15, the water quality was poor (class D for both in-situ and estimated) (table 4). This classification reflects the presence of an important level of urbanization in this region.

Univariate Analysis

Sea Surface Temperature

According to the descriptive statistics, sea surface temperature was measured in 15 locations off Morocco’s northern coast in 2017. The

[262]



TABLE 5 Descriptive Statistics of the In-Situ Measurements of the Sea Surface Temperature

Statistic elements	Values (°C)	Statistic elements	Values (°C)
Mean	23.548	Skewness	-0.197
Standard Error	1.306	Range	13.857
Median	24.437	Minimum	16.210
Standard Deviation	5.057	Maximum	30.066
Sample Variance	25.576	Sum	353.219
Kurtosis	-1.458	Count	15

[263]

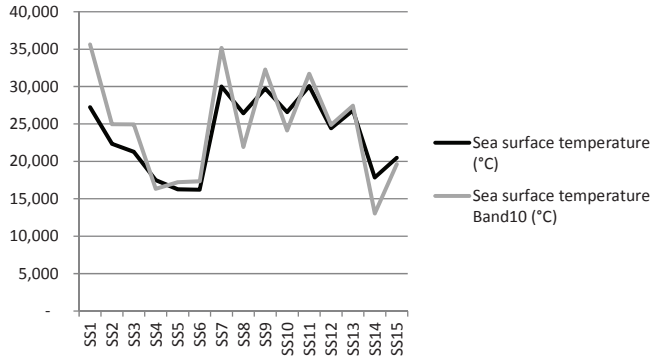
distribution of the SST is slightly skewed with a left tail (negatively asymmetric), because the median is slightly greater than the mean. In addition, the regional average of the SST is equal to 23.548 °C, and the typical deviation from this value is equal to 5.057 °C (table 5). From the comparison of the sea surface temperature of each selected site, it was observed that in 50% of the sites, the SST was smaller than 24.437 °C (table 5). It therefore represents a great deal of variability. Table 5 shows the minimum temperature in Ghandouri (16.21 °C) and the maximum temperature in Ksar-Sghir (30.066 °C).

On the other hand, we can deduce the following using the descriptive statistics of sea surface temperature estimated using the TIRS Band 10 (SST Band 10) product over the study area (table 5): First, in 2017, SST Band 10 was estimated over the same 15 sites off the northern coast of Morocco. Second, the SST Band 10 distribution is slightly skewed with a left tail (negative skew) as the median is slightly higher than the mean. Third, the regional mean of SST band 10 is 24.441 °C, and the typical deviation from this value is 7.032 °C. In addition, the SST band 10 is less than 24.883 °C in 50% of the sites. Finally, the SST band 10 has a large variability: the minimum value was estimated at Port Tangier Med (13.04 °C) and the maximum at Marqala (35.62 °C) (table 5).

We can conclude from the above that the distribution of the two sets of sea surface temperatures (measured and estimated) has the same characteristics (figure 4), similar regional values, and variability. Furthermore, because the minimum and maximum values at different locations vary, more spatial exploration is required.

[264]

FIGURE 4
Distribution
Chart of the
Sea Surface
Temperatures
(Measured and
Estimated)



E. Coli Concentrations

The concentrations of the bacteria have been measured in the same locations where the sea surface temperature was measured, and the estimated values were concluded from the same sea surface temperature measurements (Brando and Dekker 2003). Below are the descriptive statistics of the in-situ measurements of E. coli bacteria concentrations over the study region (table 6), from which we can discern that E. coli concentrations were measured in 15 sites off Morocco’s northern coast in 2017. The results indicate that the distribution of the concentration is slightly skewed with a right tail (positively asymmetric), because the mean is slightly greater than the median, while the regional average of the concentration is equal to 1047.667 UFC/100 mL and the typical deviation from this value is equal to 1189.707 UFC/100 mL (table 6). Additionally, the concentration is smaller than 880 (UFC/100 mL) in 50% of the sites, and the concentration has a great deal of variability: the minimum value was observed in Tangier City (14 (UFC/100 mL)) and the maximum in Lamrissat (4500 (UFC/100 mL)) (table 6).

Furthermore, table 6 displays descriptive statistics of the estimated concentrations of E. coli bacteria across the study region, from which we can deduce the following: in 2017, the concentration of E. coli bacteria was estimated at 15 sites off Morocco’s northern coast. Moreover, the distribution of the concentration is slightly skewed with a right tail (positively asymmetric), because the mean is slightly greater than the median. Additionally, the regional aver-



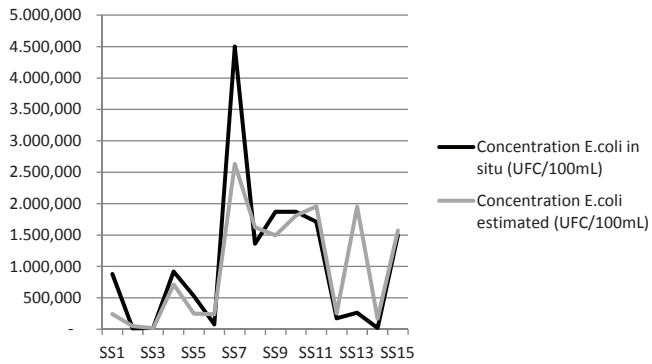
Assessment of Coastal Water Quality

TABLE 6 Descriptive Statistics of In-Situ Measurements of the E. Coli Bacteria

Statistic elements	Values (UFC/100mL)	Statistic elements	Values (UFC/100mL)
Mean	1047.667	Skewness	1.821
Standard Error	307.181	Range	4486
Median	880	Minimum	14
Standard Deviation	1189.707	Maximum	4500
Sample Variance	1415402	Sum	15715
Kurtosis	4.376	Count	15

[265]

FIGURE 5
Distribution
Chart of the E.
Coli Concentra-
tions (Measured
and Estimated)



age of the concentration is equal to 998.366 UFC/100 mL, and the typical deviation from this value is equal to 886.569 UFC/100 mL (table 6). In 50% of the sites, the concentration is smaller than 712.146 UFC/100 mL, and the concentration has a great deal of variability: the minimum value was estimated in Tangier City (19.881 UFC/100 mL) and the maximum in Lamrissat (2631.436 UFC/100 mL) in 50% of the sites (table 6). The conclusion that we can draw from this section is that the measured and estimated values' distributions are very similar in terms of proximate range, regional values, and variability. Concerningly, the minimum and maximum value locations are the same and hence, further spatial exploration needs to be conducted.

More generally, both sets of sea surface temperatures and the E. coli concentrations have conformity (figure 5), while the mean is dragged in the direction of the extreme values, and because the sets

are correlated (Brando and Dekker 2003), the distributions are the same even if the sets have opposite skewness.

Bivariate Analysis

[266] From figure 6 (left), where the SST variables' matrix is illustrated, correlation of these variables is extremely high (88.5%), we can conclude that there is an association between them, which is proven by the root mean square error ($RMSE = 0.885$). Though it was expected to have a positive association, because the correlation had previously been proven (Cherif et al. 2019), temperatures on the shore are being inspected in addition, where E. coli concentrations are probed and are more sensitive. The SST variable increases with the SST Band 10 variable. The scatterplot of these relationships also emphasizes the conclusion that there is a strong association between measured and estimated sea surface temperatures.

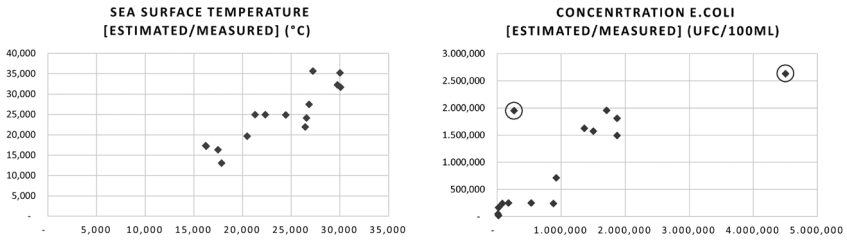
While figure 6 (right) showed that the relationship between measured and estimated E. coli concentrations is not quite linear, it could be if the two anomalies (SS5 and SS15) are ignored. Thus, in this situation, the correlation coefficient is not enough to determine the relationship between the measured and estimated concentrations over the northern shore. This means that the adequacy of this coefficient to represent the strength of the relationship is not valid. Even though the relationship is not linear, the bacterial concentrations' association is extremely high (80%); after exploring the matrix correlation of these variables, we conclude that the ($RMSE = 0.8$), which means that there is an association between them, but the nature of this association is not clear. The concentrations of E. coli are indeed sensitive to water temperature, but further parameters need to be inspected and analyzed before we can draw any conclusions.

Exploratory Spatial Data Analysis

Data Posting and Regional Histograms

The following section illustrates the use of the spatial aspect of the sites, by data posting (arc GIS) to graphically investigate our dataset and gain a better understanding of it. From the data posting maps





[267]

FIGURE 6 Scatterplot Illustrating the Association of: (left) SST Measured and Estimated (x: Measured, y: estimated); (right) Concentration of E. Coli Measured and Estimated (Anomalies: Circle)

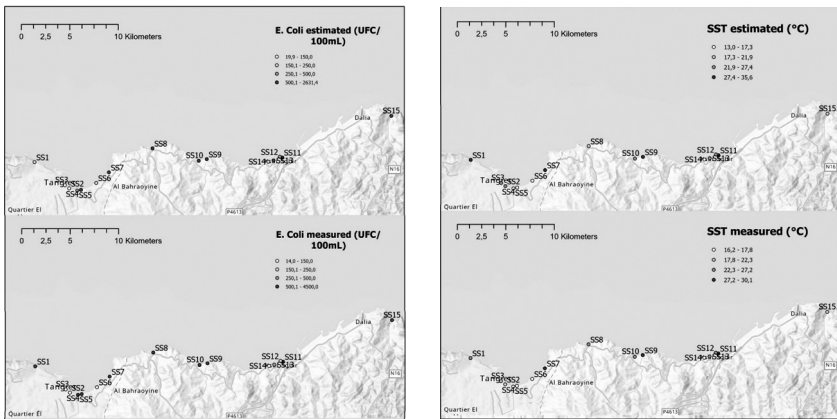


FIGURE 7 Spatial Distribution of SST and E. Coli Concentration (Ranges of the Scale Depict the Water Quality Index A–D)

(figure 7), we can extract some spatial distribution information; a relative spatial correlation between the estimated and measured values can be noted. The higher concentrations of the E. coli and temperature were located near the estuaries. Moreover, there is no apparent trend over the study area.

Regional histograms of both sets of variables were produced to further explore the spatial association of the data (figure 8). The range of values for each histogram is separated into eight classes. Histograms indicate that the data is unimodal, asymmetric, and relatively heterogeneous. The left tail of the distribution of the E. coli concentration histograms indicates the presence of a few sample points with low values.

[268]

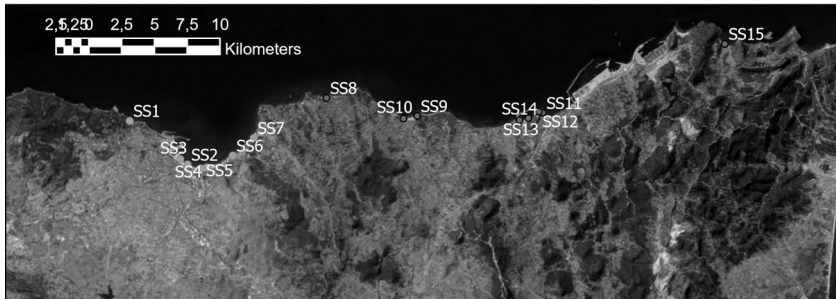
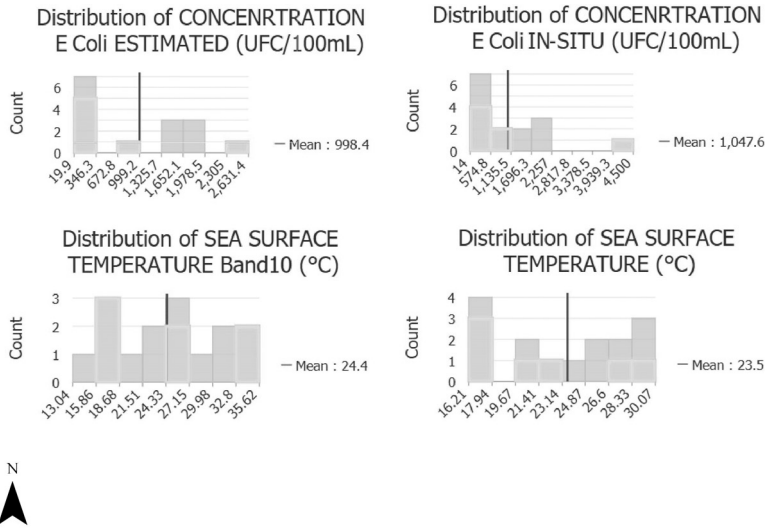


FIGURE 8 Indicator Map of the Selected Sites and Their Distribution Over the Regional Histograms (Estimated on the Left, Measured on the Right)

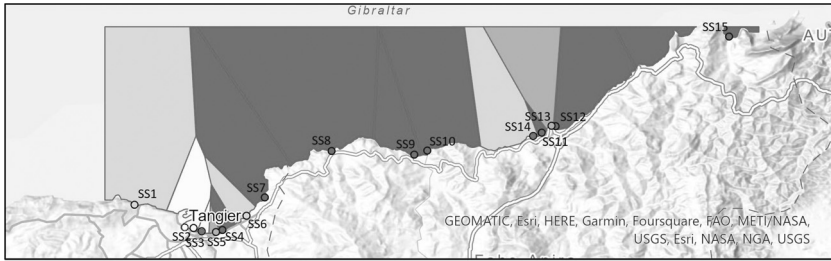
When sites on the map are selected, we can investigate if we have a spatial regime around the biggest city, Tangier. We can conclude that we have no proportional effect in the Tangier area, because the points are spread throughout the histogram.

Voronoi Map and Local Moran's I Statistics

To visualize the variation in E. coli concentration at each point using the Voronoi map (figure 9), we used it in spatial statistics analysis to investigate the variation of each point in relation to its surroundings, meaning that instead of depending on the points' loca-



Assessment of Coastal Water Quality



[269]

CONCENTRATION E.Coli ESTIMATED (UFC/100mL)

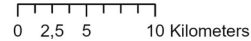
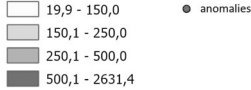


FIGURE 9 Voronoi Map of the E. Coli Concentrations in the Study Area

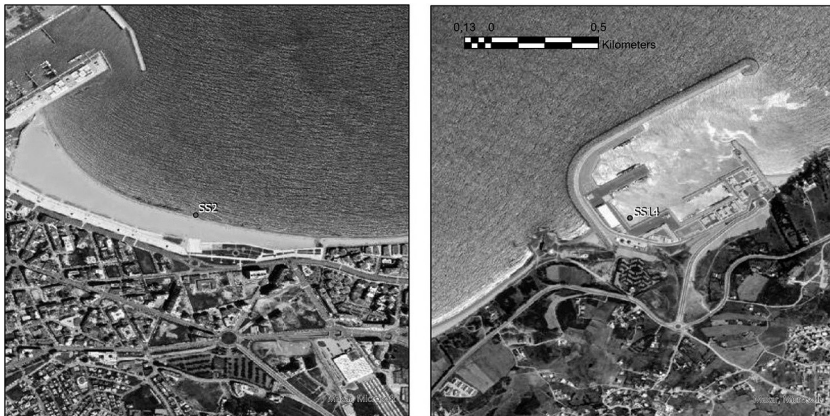
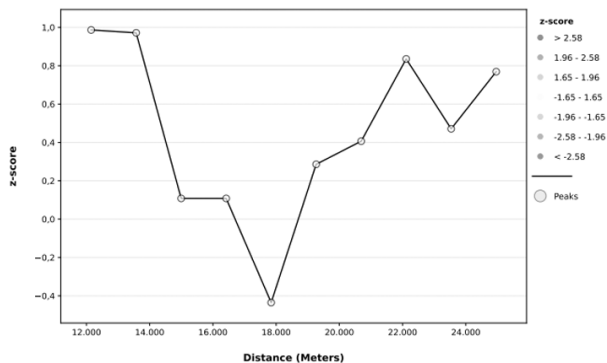


FIGURE 10 Location of the Voronoi Anomalies in the Study Area

tions, it depends on the distance between them. A conclusion can be drawn from visualizing our produced Voronoi map of the estimated E. coli concentrations; the spatial distribution seems homogeneous overall in the study region, where the spatial autocorrelation pattern tends more to anisotropy with the major continuity direction in the east/west. We will assume that the concentrations estimated are isotropic so that we can model the global spatial autocorrelation, because the anisotropy patterns cannot be modeled. The highest values are in the center. The lowest values are near Tangier. No

[270]

FIGURE 11
Spatial Autocorrelation of the Estimated E. coli Concentrations by Distance (z-Scores of the Local Moran's I Statistic)



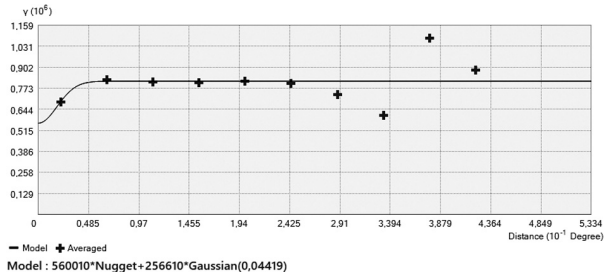
apparent trend is visible over the study domain. There are two outliers: the first site is proximate to a small port, and the second falls directly on a marine outfall (figure 10). The 15 sites selected were subject to a visual inspection, thus we can assume that the two sites with anomalies are more susceptible, which explains that the fluctuating variance of the bacterial concentrations is due to proximity to hazardous emissions. Nevertheless, the data used is very scarce, and more sample sites are needed to conduct further statistical investigations and draw a clearer conclusion.

We used inverse distance squared (Maleika 2020) for the conceptualization of spatial relationships considering the continuous nature of the concentrations (estimated), and using the incremental spatial autocorrelation tool to select an appropriate threshold distance, we constructed a line graph of the distances and their corresponding z-scores of the local Moran's I statistic. The peak z-scores indicate distances where spatial processes promote clustering; these are the appropriate values to use in tools that require a distance band or threshold distance parameter.

As a result, we got 3 statistically significant peaks (figure 11); clustering is pronounced at each of those distances, which correspond to a statistically significant peak at 12000 m, 12800 m, and 22000 m, respectively. According to these values, we can indicate that there were no spatial outliers nor clusters of low or high values (though we considered taking the second peak); all the points are not statistically significant, which means that we do not have enough evi-



FIGURE 12
Semi-Variogram Model of the Estimated E. Coli Concentrations by Distance



[271]

dence to reject the ‘complete spatial randomness’ hypothesis, which is justified by the figure that the E. coli concentration can be affected by the distance.

Inverse Distance Weighting (IDW)

To fit a model using the predicted and error graphs, and the summary information on prediction errors, as well as by examining pairs of measured and predicted values, we got the semi-variogram in figure 12. With the model (560010*Nugget + 256610*Gaussian (0.04419)), with the respective parameters (Nugget: 560010; Partial Sill: 256610; Major Range: 0.04419°), these parameters characterize the model’s function represented by the line in figure 12. The magnitude of the RMSE (Root Mean Square Error) values did not change much, except where the last values (averaged) are concerned, which are presented in a value range of 2.91 to 4.364, indicating that the mean error is not close to zero in all observations.

The IDW utilizes values around the prediction location and can predict values for unsampled locations accordingly, assuming that ‘things that are close to one another are more related than things that are farther apart’ (El Azhari et al. 2022; Masoudi 2021). 15 points were taken to observe the E. coli concentration in the Tangier Ksar-Sghir Region in 2017 and were used as sample points to interpolate the surrounding E. coli concentration. This is presented in the IDW prediction map framing the northern coast of Morocco (figure 13), which respectively represents the bathing water quality.

The purpose of this study was to present the results of the IDW for the spatial distribution of the E. coli concentration data in the Tangier Ksar-Sghir region. The lower values on the map represent

[272]

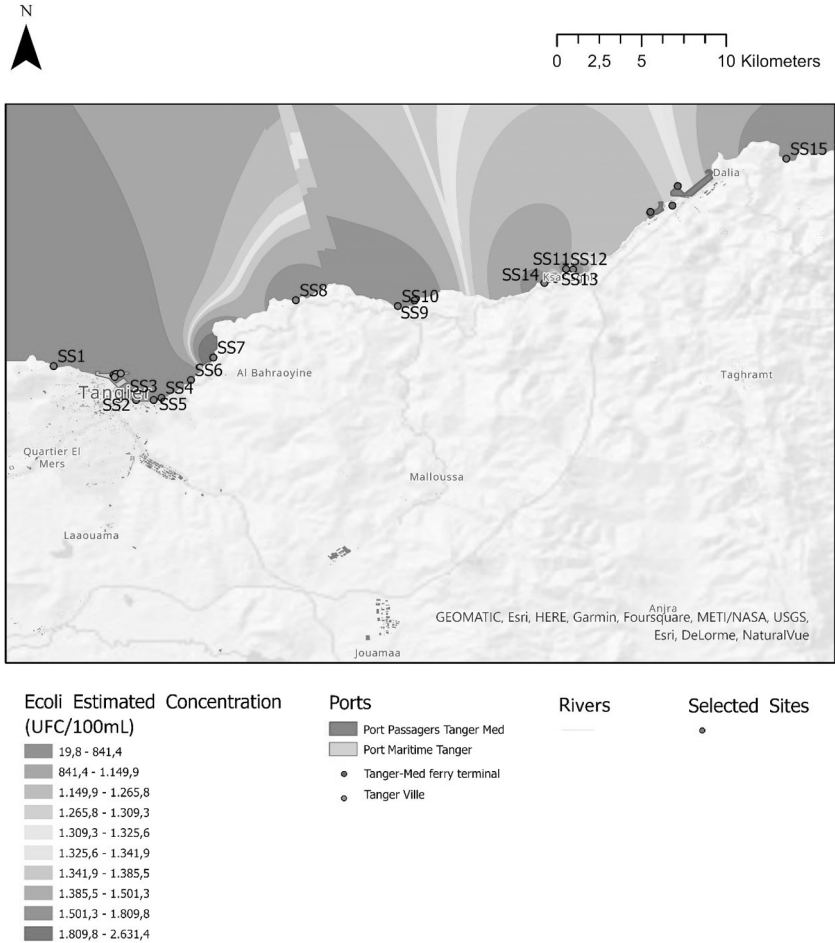


FIGURE 13 Predicted Surface of the Estimated E. coli Concentrations Using Inverse Distance Weighting (IDW)

low levels of E. coli concentrations in nine samples, which account for 60% of the samples, while the higher values represent higher amounts of pollution detected in the samples (SS7, SS8, SS9, SS10, SS12, and SS15), the maximum being in sample SS7 with an average (from 1809.8 to 2637.4) of estimated E. coli concentration. From the results, we can conclude that only values near the shore are valid, while the values deeper in the Gibraltar Strait were extrapolated due to the absence of data points in depth (Cherif and Salmoun 2017).



Tangier Med Port was established in 2016 and it has significantly changed the landscape (Jebbad et al. 2022); for instance, in just one year, it relieved one of the most heavily trafficked ports in northern Africa, Maritime Tangier Port, which directly implies the accumulation of pollution from routine ship spills, including garbage and fuel (Er-Raioui et al. 2012). As it is possible to see, around the Tangier-Med port there are much higher values of pollution (Luigia et al. 2020), as well as around the estuaries. This is explained by the presence of runoff from agriculture, industry, and sewage, rich in waste, that settle in the sediments of the shore in these regions, which increases the pollution levels registered there. The city of Tangier has the lowest values in the study region.

[273]

Nowadays, remote sensing made it possible to forecast the quality of coastal waters. Through our study, we have demonstrated the potential of Landsat 8, which provides useful information at a high spatial resolution (100 m) for the identification of coastal water pollution.

Furthermore, the strategic methodology applied in this study goes beyond the limits of the current norm, which assesses microbiological quality based solely on viable bacteria enumerated at fixed stations within the bathing zone. By using the methodology (Cherif et al. 2020), the concentration of *E. coli* could directly be determined from the difference between Sea Surface Temperature (SST) and Air Temperature (AT). This method was applied and tested on the Atlantic coast of Tangier and the western entrance to the Strait of Gibraltar, and could be used in any location which suffers from similar environmental problems.

Generally, to improve the performance of remote sensing, it will be necessary to simulate the dynamics of different physiological states of *E. coli* populations in response to physico-chemical fluctuations.

CONCLUSION

In the perspective of environmental protection, this study aims to contribute to the establishment of a coastal monitoring system, the development of new management solutions, and the implementa-

[274] tion of the functionality of *Escherichia coli* (*E. coli*), as an indicator in prediction, of the marine pollution phenomena. The development of forecasting systems will allow local authorities to identify specific mitigation measures at the right time, thus reducing the risks to bathers' health coming from fecal bacteria.

The concretization of this project was important to further apply our knowledge of spatial statistics tools and use the spatial aspect of the data that has been hitherto untreated. The application of these tools helped us understand the relationship between the different variables, and the contrasts in the levels of bacterial propagation in the northern shore of Morocco.

The results of the present study showed low *E. coli* concentrations and SST values in Tangier City (SS1, SS2 and SS3), and Ksar-Sghir (SS14). In addition, the high values of *E. coli* concentrations and SST values at SS4–SS13 and SS15 can be attributed to discharge from the Souani and Mghogha rivers, and rejections from ships (marine traffic) in Tangier Med Port. Therefore, a significant correlation was found between the remote sensing temperature from Landsat 8 images and different bacteriological parameters. Indeed, the tested equation previously developed for use in the western Atlantic coast of Tangier (Cherif et al. 2020), proved a great result determining the quality of the Mediterranean northern coastal waters of Tangier.

Compared to traditional methods, remote sensing is one of the best tools for providing interesting information to decision makers based on sensed water temperature data. It can provide high temporal and spatial resolution information for the assessment and regular monitoring of this region's marine environment. Therefore, the regression model provides evaluation and detection of potential pollution along the coast, which is represented by an R^2 of 80%. Moreover, the IDW showed that the region of pollution is correlated with the discharge and port zones. Only values near the shore are valid, while the values deeper in the Gibraltar Strait were extrapolated due to the absence of data points at depth.

The present study should be taken as a preliminary result, and these results may be relevant to areas with similar characteristics as Morocco and elsewhere. In perspective, other analyses, such as



heavy metals and other bacteriological analyses, are necessary to develop a control approach to limit the negative impacts of seawater pollution in the context of sustainable development and the preservation of water resources. Overall, the results will support decision makers in establishing adequate policies to prevent environmental hazards and achieve good water quality along the coast of Tangier Ksar-Sghir, Morocco, in the future. [275]

ACKNOWLEDGMENTS

Conceptualization, E. K. C. and H. B.; methodology, E. L. C., Y. E.; software, Y. E. and A. B.; validation, E. K. C. and H. B.; formal analysis, Y. E. and A. B.; writing—original draft preparation, E. L. C., Y. E. and A. B.; writing—review and editing, E. A. H., Y. E., H. E. A., and A. B.; visualization, A. B.; supervision, E. K. C. and H. B.; funding acquisition, E. K. C. All authors have read and agreed to the published version of the manuscript.

The authors would like to thank all the collaborators within this work, from the Field sampling, laboratory analysis and writing manuscript team. We would like to thank Alexandre Bernardino for his advices and support.

REFERENCES

- Alparslan, E., C. Aydoğan, V. Tufekci, and H. Tufekci. 2007. 'Water Quality Assessment at Ömerli Dam Using Remote Sensing Techniques.' *Environmental Monitoring and Assessment* 135:391–98.
- Amani, M., A. Moghimi, S. M. Mirmazloumi, B. Ranjgar, A. Ghorbanian, S. Ojaghi, H. Ebrahimi, A. Naboureh, M. E. Nazari, and S. Mahdavi. 2022. 'Ocean Remote Sensing Techniques and Applications.' *Water* 14:3400.
- Anding, D., and R. Kauth. 1970. 'Estimation of Sea Surface Temperature from Space.' *Remote Sensing of Environment* 1:217–20.
- Banzon, V., T. M. Smith, T. M. Chin, C. Liu, and W. Hankins. 2016. 'A Long-Term Record of Blended Satellite and in Situ Sea-Surface Temperature for Climate Monitoring, Modeling and Environmental Studies.' *Earth System Science Data* 8 (1): 165–76.
- Ben Ali, M., and A. Mahacine. 2022. 'Assessment of the Environmental Impact of the Tangier Med Port by the Cause-Effect Method.' *IOSR Journal of Engineering* 16 (4): 31–9.
- Bouramtane, T., I. Kacimi, K. Bouramtane, M. Aziz, S. Abraham, K. Omari, and L. Barbiero. 2021. 'Multivariate Analysis and Machine Learning Approach for Mapping the Variability and Vulnerability of Urban Flooding: The Case of Tangier City, Morocco.' *Hydrology* 8 (4): 182.
- Bourouhou, I., and F. Salmoun. 2021a. 'A Study on the Bacteriological Characterization of the Coastal Tangier Seawater: Preliminary Results.' *E3S Web of Conferences* 234:00014.

- Bourouhou, I., and F. Salmoun. 2021b. 'Sea Surface Temperature Estimation Using Remotely Sensed Imagery of Landsat 8 along the Coastline of Tangier-Ksar-Sghir Ksar-Sghir Region.' *E3S Web of Conferences* 234:00096.
- Brando, V. E., and A. G. Dekker. 2003. 'Satellite Hyperspectral Remote Sensing for Estimating Estuarine and Coastal Water Quality.' *IEEE Transactions on Geoscience and Remote Sensing* 41:1378–87.
- Bradtke, K. 2021. 'Landsat 8 Data as a Source of High Resolution Sea Surface Temperature Maps in the Baltic Sea.' *Remote Sensing* 13:4619.
- Cheng, K. H., J. J. Jiao, X. Luo, and S. Yu. 2022. 'Effective Coastal *Escherichia Coli* Monitoring by Unmanned Aerial Vehicles (UAV) Thermal Infrared Images.' *Water Research* 222:118900.
- Cherif, E., and F. Salmoun. 2017. 'Contribution of Remote Sensing and Bacteriological Analysis for the Quality of Bathing Waters on the West Coast of Tangier.' Paper presented at the Coastal and Maritime Mediterranean Conference, Split.
- Cherif, E. K., F. Salmoun, and F. J. Mesas-Carrascosa. 2019. 'Determination of Bathing Water Quality Using Thermal Images Landsat 8 on the West Coast of Tangier: Preliminary Results.' *Remote Sensing* 11:972.
- Cherif, E. K.; M. Vodopivec, N. Mejjad, J. C. Silva, S. Simonovič, and H. Boulaassal. 2020. 'COVID-19 Pandemic Consequences on Coastal Water Quality Using WST Sentinel-3 Data: Case of Tangier, Morocco.' *Water* 12:2638.
- Doña, C., N.-B. Chang, V. Caselles, J. M. Sánchez, L. Pérez-Planells, M. D. M. Bisquert, V. García-Santos, S. Imen, and A. Camacho. 2016. 'Monitoring Hydrological Patterns of Temporary Lakes Using Remote Sensing and Machine Learning Models: Case Study of La Mancha Húmeda Biosphere Reserve in Central Spain.' *Remote Sensing* 8:618.
- Doney, S. C. 2010. 'The Growing Human Footprint on Coastal and Open-Ocean Biogeochemistry.' *Science* 328 (5985): 1512–6.
- Donlon, C. J., M. Martin, J. Stark, J. Roberts-Jones, E. Fiedler, and W. Wimmer. 2012. 'The Operational Sea Surface Temperature and Sea Ice Analysis (OSTIA) System.' *Remote Sensing of Environment* 116:140–58.
- El Azhari, H., E. K. Cherif, O. Sarti, E. M. Azzirgue, H. Dakak, H. Yachou, J. C. G. Esteves da Silva, and F. Salmoun, F. 2022. 'Assessment of Surface Water Quality Using the Water Quality Index (IWQ), Multivariate Statistical Analysis (MSA) and Geographic Information System (GIS) in Oued Laou Mediterranean Watershed, Morocco.' *Water* 15 (1): 130.
- El-Din, M. S., A. Gaber, M. Koch, R. S. Ahmed, and I. Bahgat. 2013. 'Remote Sensing Application for Water Quality Assessment in Lake Timсах, Suez Canal, Egypt.' *Journal of Remote Sensing Technology* 1 (3): 61–74.
- Er-Raioui, H., S. Khannous, M. O. Mohamed Cheihk, M. Mhamada, and



- S. Bouzid. 2012. 'The Moroccan Mediterranean Coastline: A Potential Threatened by the Urban Discharges.' *The Open Environmental Pollution & Toxicology Journal* 3:23–36.
- Galve, J. M., J. M. Sánchez, V. García-Santos, J. González-Piqueras, A. Calera, and J. Villodre. 2022. 'Assessment of Land Surface Temperature Estimates from Landsat 8-TIRS in A High-Contrast Semiarid Agroecosystem: Algorithms Intercomparison.' *Remote Sensing* 14 (8): 1843.
- Gholizadeh, M. H., M. M. Assefa, and R. A. Lakshmi. 2016. 'A Comprehensive Review on Water Quality Parameters Estimation Using Remote Sensing Techniques.' *Sensors* 16:1298.
- Giardino, C., M. Bresciani, I. Cazzaniga, K. Schenk, P. Rieger, F. Braga, E. Matta, and V. E. Brandò. 2014. 'Evaluation of Multi-Resolution Satellite Sensors for Assessing Water Quality and Bottom Depth of Lake Garda.' *Sensors* 14:24116–31.
- Gómez, F. 2003. 'The Role of the Exchanges through the Strait of Gibraltar on the Budget of Elements in the Western Mediterranean Sea: Consequences of Human-Induced Modifications.' *Marine Pollution Bulletin* 46:685–94.
- Gong, S., H. Wang, Z. Zhu, Q. Bai, and C. Wang. 2019. 'Comprehensive Utilization of Seawater in China: A Description of the Present Situation, Restrictive Factors and Potential Countermeasures.' *Water* 11:397.
- Govekar, P. D., C. Griffin, and H. Beggs. 2022. 'Multi-Sensor Sea Surface Temperature Products from the Australian Bureau of Meteorology.' *Remote Sensing* 14:3785.
- Grau, E., and J. P. Gastellu-Etchegorry. 2013. 'Radiative Transfer Modeling in the Earth-Atmosphere System with DART Model.' *Remote Sensing of Environment* 139:149–70.
- Gravari-Barbas, M., and S. Jacquot. 2018. *Atlas Mondial Du Tourisme et Des Loisirs: Du Grand Tour Aux Voyages Low Cost*. Paris: Autrement.
- Hadjimitsis, D. G., and C. Clayton. 2009. 'Assessment of Temporal Variations of Water Quality in Inland Water Bodies Using Atmospheric Corrected Satellite Remotely Sensed Image Data.' *Environmental Monitoring and Assessment* 159:281–92.
- Haut Commissariat au Plan. 2020. *Monographie de la région Tanger-Tetouan-Al Hoceima*. N. p.: Haut Commissariat au Plan.
- Islam, M. S., and M. Tanaka. 2004. 'Impacts of Pollution on Coastal and Marine Ecosystems Including Coastal and Marine Fisheries and Approach for Management.' *Marine Pollution Bulletin* 48 (7–8): 624–49.
- Jebbad, R., J. P. Sierra, C. Mösso, M. Mestres, and A. Sánchez-Arcilla. 2022. 'Assessment of Harbour Inoperability and Adaptation Cost Due to Sea Level Rise. Application to the Port of Tangier-Med (Morocco).' *Applied Geography* 138:102623.

- Kondratyev, K. Y., D. Pozdnyakov, and L. Pettersson. 1998. 'Water Quality Remote Sensing in the Visible Spectrum.' *International Journal of Remote Sensing* 19:957-79.
- Lamghari Moubarrad, F.-Z., and O. Assobhei. 2005. 'The Health Effects of Wastewater on the Prevalence of Ascariasis among the Children of the Discharge Zone of El Jadida, Morocco.' *International Journal of Environmental Health Research* 15:135-42.
- Luigia, M., F. Murena, F. Quaranta, and D. Toscano. 2020. 'A Methodology for the Design of an Effective Air Quality Monitoring Network in Port Areas.' *Scientific Reports* 10:300.
- Mahjoubi, F. K. 2019. 'Evaluation of Water Quality of Oum Er Rbia River (Morocco) Using Water Quality Index (WQI) Method.' *Journal of Applied Surfaces and Interfaces* 5 (1-3): 1-12.
- Maillard, P., and N. A. P. Santos. 2008. 'A Spatial-Statistical Approach for Modeling the Effect of Non-Point Source Pollution on Different Water Quality Parameters in the Velhas River Watershed - Brazil.' *Journal of Environmental Management* 86:158-70.
- Maleika, W. 2020. 'Inverse Distance Weighting Method Optimization in the Process of Digital Terrain Model Creation Based on Data Collected from a Multibeam Echosounder.' *Applied Geomatics* 12:397-407.
- Masoudi, M. 2021. 'Estimation of the Spatial Climate Comfort Distribution Using Tourism Climate Index (TCI) and Inverse Distance Weighting (IDW) (Case Study: Fars Province, Iran).' *Arabian Journal of Geosciences* 14:363.
- Maul, G. A., and I. W. Duedall. 2019. 'Demography of Coastal Populations.' In *Encyclopedia of Coastal Science*, edited by C. W. Finkl and C. Makowski, 692-700. Cham: Springer.
- Morgan, B. J.; M. D. Stocker, J. Valdes-Abellan, M. S. Kim, and Y. Pachep-sky. 2020. 'Drone-Based Imaging to Assess the Microbial Water Quality in an Irrigation Pond: A Pilot Study.' *Science of the Total Environment* 716:135757.
- Odonkor, S. T., and T. Mahami. 2020. 'Escherichia Coli as a Tool for Disease Risk Assessment of Drinking Water Sources.' *International Journal of Microbiology* 2020:2534130.
- Peng, X., S. Feng, S. Lai, Z. Liu, J. Gao, M. Javanbakht, and B. Gao. 2022. 'Structural Engineering of Rare-Earth-Based Perovskite Electrocatalysts for Advanced Oxygen Evolution Reaction.' *International Journal of Hydrogen Energy* 47:39470-85.
- Pyo, J. C., S. H. Ha, Y. A. Pachepsky, H. Lee, R. Ha, G. Nam, S. K. Moon, I. Jung-ho, and H. C. Kyung. 2016. 'Chlorophyll-a Concentration Estimation Using Three Difference Bio-Optical Algorithms, Including a Correction for the Low-Concentration Range: The Case of the Yiam Reservoir, Korea.' *Remote Sensing Letters* 7:407-16.



- Ramdani, F., A. Wirasatriya, and A. R. Jalil. 2021. 'Monitoring The Sea Surface Temperature and Total Suspended Matter Based on Cloud-Computing Platform of Google Earth Engine and Open-Source Software.' *IOP Conference Series: Earth and Environmental Science* 750:012041.
- Ritchie, J. C., P. V. Zimba, and J. H. Everitt. 2003. 'Remote Sensing Techniques to Assess Water Quality.' *Photogrammetric Engineering & Remote Sensing* 69:695–704.
- Roy, D. P., M. A. Wulder, T. R. Loveland, C. E. Woodcock, R. G. Allen, R. G., M. C. Anderson, and Z. Zhu. 2014. 'Landsat-8: Science and Product Vision for Terrestrial Global Change Research.' *Remote Sensing of Environment* 145:154–72.
- Sertel, E., B. Ekim, P. Ettehadi Osgouei, and E. Kabadayi. 2022. 'Land Use and Land Cover Mapping Using Deep Learning Based Segmentation Approaches and VHR Worldview-3 Images.' *Remote Sensing* 14:4558.
- Seyhan, E., and A. Dekker. 1986. 'Application of Remote Sensing Techniques for Water Quality Monitoring.' *Hydrobiological Bulletin* 20 (1–2): 41–50.
- Sheffield, J. 2018. 'Satellite Remote Sensing for Water Resources Management: Potential for Supporting Sustainable Development in Data-Poor Regions.' *Water Resources Research* 54:9724–58.
- Sikder, M., E. N. Naumova, A. O. Ogudipe, M. Gomez, and D. Lantagne. 2021. 'Fecal Indicator Bacteria Data to Characterize Drinking Water Quality in Low-Resource Settings: Summary of Current Practices and Recommendations for Improving Validity.' *International Journal of Environmental Research and Public Health* 18:2353.
- Sloggett, D. R., J. Aiken, M. Srokosz, and S. Boxall. 1995. *Operational Uses of Ocean Colour Data-Perspectives for the OCTOPUS Programme*. Rotterdam: Balkema.
- Teixeira Pinto, C., X. Jing, and L. Leigh. 2020. 'Evaluation Analysis of Landsat Level-1 and Level-2 Data Products Using in Situ Measurements.' *Remote Sensing* 12 (16): 2597.
- Topp, S. N., T. M. Pavelsky, D. Jensen, M. Simard, and M. R. V. Ross. 2020. 'Research Trends in the Use of Remote Sensing for Inland Water Quality Science: Moving Towards Multidisciplinary Applications.' *Water* 12:169.
- Usali, N., and M. H. Ismail. 2010. 'Use of Remote Sensing and GIS in Monitoring Water Quality.' *Journal of Sustainable Development* 3:228–38.
- Vanhellemont, Q. 2020. 'Automated Water Surface Temperature Retrieval from Landsat 8/TIRS.' *Remote Sensing of Environment* 237:111518.
- US Geological Survey. 2019. *Landsat 8: Data Users Handbook*. Sioux Falls, SD: US Geological Survey.
- . 2023a. *Landsat: Atmospheric Auxiliary Data; Data Format Control Book (DFCB)*. Sioux Falls, SD: US Geological Survey.

———. 2023b. *Landsat 8–9: Collection 2 (C2); Level 2 Science Product Guide*.
Sioux Falls, SD: US Geological Survey.

Wang, X., and T. Ma. 2001. 'Application of Remote Sensing Techniques in
Monitoring and Assessing the Water Quality of Taihu Lake.' *Bulletin of
Environmental Contamination and Toxicology* 67:863–70.

[280]

Wu, Z., G. Snyder, C. Vadnais, R. Arora, M. Babcock, G. Stensaas, P. Doucette,
and T. Newman. 2019. 'User Needs for Future Landsat Missions.' *Re-
mote Sensing of Environment* 231:111214.

Yang, H., J. Kong, H. Hu, Y. Du, M. Gao, and F. Chen. 2022. 'A Review of
Remote Sensing for Water Quality Retrieval: Progress and Challenges.'
Remote Sensing 14:1770.

Yi, L., S. Ma, S. Tao, J. Zhang, and J. Wang. 2022. 'Coastal Landscape Pat-
tern Optimization Based on the Spatial Distribution Heterogeneity of
Ecological Risk.' *Frontiers in Marine Science* 9:1003313.

